PREPARATION OF SODIUM SILICATE SOLUTIONS AND SILICA NANOPARTICLES FROM SOUTH AFRICAN COAL FLY ASH

Mathibela E. Aphane[1,2], Frédéric J. Doucet[3]*, Richard A. Kruger[4], Leslie Petrik[5] and Elizabet M. van der Merwe[1]*

[1]*Chemistry Department, University of Pretoria, Lynnwood Road, Pretoria, 0001;*

[2]*Department of Chemistry, PO Box 392, UNISA, Pretoria, 0003, South Africa;*

[3]*Council for Geoscience, 280 Pretoria Road, Private Bag X112, Pretoria 0001, South Africa;*

[4]*Richonne Consulting, PO Box 742, Somerset Mall, 7137, South Africa*

[5]*Environmental and Nano Science Group, Department of Chemistry, University of the Western Cape, Private Bag X17, Bellville 7535, South Africa*

*Co-corresponding authors: liezel.vandermerwe@up.ac.za (+27 12 420 5379);

fdoucet@geoscience.org.za (+27 12 841 1300)

ORCID:

Mathibela E. Aphane: 0000-0002-5957-5920

Frédéric J. Doucet: 0000-0002-7980-476X

Leslie Petrik: 0000-0002-2049-1551

Elizabet M. van der Merwe: 0000-0002-4452-1292

ACKNOWLEDGEMENTS

The project was financially supported by UNISA, University of Pretoria, Council for Geoscience, and the National Research Foundation of South Africa (NRF; Grant No.93641). Any opinion, finding and conclusion or recommendation expressed in this material is that of the authors and the NRF does not accept any liability in this regard. The authors thank Ms Wiebke Grote for XRD, Ms Jeanette Dykstra for XRF, University of Pretoria Laboratory for Microscopy and Microanalysis for assistance with FESEM, and Ash Resources (Pty) Ltd for providing the fly ash sample.

ABSTRACT

The production of amorphous mesoporous silica nanoparticles can be achieved using sodium silicate (Na_2SiO_3) solutions prepared from South African coal fly ash waste. The first part of this study compared two processes for the preparation of Na_2SiO_3 solutions. The first process, hereafter called sequential acid-alkaline leaching (SAAL), is a two-stage process, which involves (i) a H_2SO_4 leaching step for the preferential extraction of reactive aluminium over silicon, followed by (ii) the preferential extraction of silicon over aluminium from the resulting residues using NaOH. The second process is a direct alkaline leaching (DAL) process, which consists of a single-stage elemental extraction from ash using NaOH, *i.e.* without the preceding acid leaching step used in SAAL. The two processes generated Na_2SiO_3 solutions with identical pH (11.8), similar silicon (10.2-10.3 g/L), iron (*ca.* 200 mg/L) and potassium (*ca.* 800 mg/L) content, and low calcium concentrations (≤ 29 mg/L). However, the inclusion of the acid leaching step in the SAAL process yielded a Na_2SiO_3 solution with significantly lower aluminium content (166 mg/L *vs* 1158 mg/L). The Na_2SiO_3 solutions obtained from the SAAL and DAL processes were then used as silica precursors to synthesise silica nanoparticles via a sol-gel method using polyethylene glycol (PEG) as surfactant and sulphuric acid as catalyst. All samples of synthesised silica nanoparticles were characterised by a high level of purity (up to 99.3 wt% SiO_2). The insight gained is now being used to improve existing processes for the production of high-grade ultra-pure silica nanoparticles (*i.e.* ≥ 99.9 wt% SiO_2) for catalyst support applications.

GRAPHICAL ABSTRACT

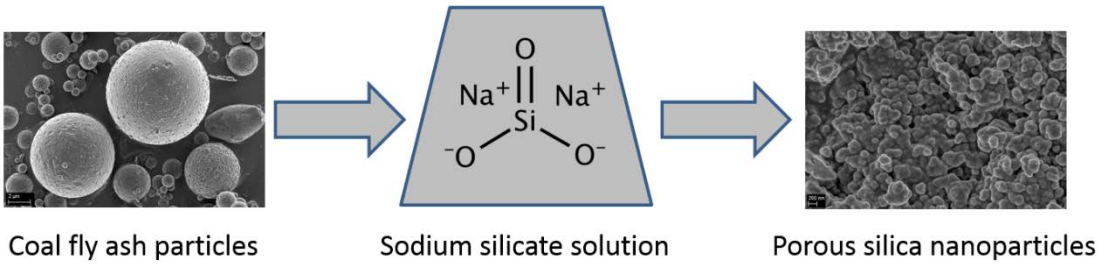

KEYWORDS: coal fly ash, extraction, aluminium, silicon, sodium silicate, silica nanoparticles

STATEMENT OF NOVELTY

This paper successfully demonstrates the synthesis of amorphous mesoporous silica nanoparticles from sodium silicate solutions which were prepared from a South African classified coal fly ash. Two processes for the preparation of Na_2SiO_3 solutions were tested and compared in order to assess whether pre-treatment for the removal of reactive aluminium from ash is beneficial to SiO_2 nanoparticles synthesis. Na_2SiO_3 solutions prepared using the two processes were then used as silica precursors to synthesise silica nanoparticles via a sol-gel method. The insight gained is now being used to improve existing processes for the production of high-grade ultra-pure silica nanoparticles, while the pure nanoparticles synthesised in this study are currently being tested for catalyst support applications.

1. Introduction

Coal fly ash (CFA) is a by-product generated during the combustion of pulverised coal in thermoelectric power stations. South Africa's public electricity utility, Eskom, consumes about 120 million tons of coal per annum, which produces 34 million tons of CFA [1]. Only about 5% of South African CFA is recycled, mostly in the cement and construction industry. Current legislative requirements impose stringent measures to be in place for ash storage facilities, which result in expensive management practices.

Due to its high silicon (Si) and aluminium (Al) content, South African CFA could represent valuable secondary resource of purified silica and alumina, provided suitable economically-viable processes can be developed. The economic importance of silica nanoparticles is evidenced by its widespread inclusion in various industrial applications. Examples of applications include catalysts and catalyst supports, pigments, electronic substrates, thin film substrates, electrical and thermal insulators, filters for exhaust gases, and adsorbents [2–7].

Numerous synthetic methods for the preparation of silica nanoparticles have been proposed, including vapour-phase reactions, sol–gel synthesis, thermal decomposition techniques, and ammonification [8–10]. The sol-gel technique presents many processing merits, mainly due to its versatility and the ease by which modification of material properties may be achieved by changing synthesis parameters [11]. It is cost-effective and produces homogeneous and non-toxic silica particles of high purity [12]. Although alkyl orthosilicates are the most commonly used silica source, their high cost, flammability, and difficulties in handling and storage call for alternative sources [13]. Aqueous

solutions of Na_2SiO_3 are known to be alternative silica sources for the production of silica nanoparticles via the sol-gel synthetic process [14–16].

Commercial preparation of Na_2SiO_3 solutions is achieved by reacting SiO_2-containing material, such as quartz sand, with carbonates or sulphates of alkali metals at temperatures exceeding 1300°C, with subsequent dissolution in water below 200°C for several hours [17]. This synthesis route is energy-intensive and generates carbon dioxide and sulphur trioxide emissions that must be managed, which make the synthesis of silica nanoparticles expensive [18]. The development of simple, affordable, and low-energy methods for the production of Na_2SiO_3 solutions is therefore needed. For instance, Na_2SiO_3 solutions have been prepared from the reaction of commercial amorphous silica with NaOH solution at 90°C [19]. However, the starting SiO_2 source can also be obtained from widely-available waste materials.

Preparation of Na_2SiO_3 solutions from solid waste materials using acidic and/or alkaline leaching processes has been the subject of several studies. Examples of solid waste materials that have been investigated include rice hull ash [20,21], rice straw ash [5], bagasse ash [22], and oil shale ash [23]. Na_2SiO_3 solutions have also been prepared from CFA. The methods discussed in the literature generally involve an acid leaching pre-treatment step with the purpose of removal of Al and other elements as impurities from the solid waste material, followed by a NaOH leaching step to selectively extract Si in preparation of the Na_2SiO_3 solution, although their reported efficiency vary somewhat owing to differences in mineralogy and reactivity between coal ashes generated in different countries from various coals and combustion conditions. For instance, 37.3% [24] up to 62% SiO_2 [25] were extracted from Chinese CFA via leaching in 20-30 % w/w NaOH solution at 100-125°C for 1-2 h. Na_2SiO_3 solutions were also generated from Malaysian CFA via alkali fusion at 550°C followed by aqueous dissolution [26]. In South Africa, the preparation of Na_2SiO_3 from CFA is limited to a single study for oil well cement applications using an non-classified (≤ 112 µm) ash sample from a non-specified power station [27].

The primary objective of this paper was to demonstrate the successful production of SiO_2 nanoparticles from a South African classified CFA. A second objective was to test whether the removal of reactive aluminium from CFA prior to silicon extraction for the production of intermediate Na_2SiO_3 solutions is beneficial to SiO_2 nanoparticles synthesis.

2. Experimental

2.1 Materials tested and chemical reagents

A representative sample of a classified, ultrafine siliceous CFA sample was obtained from Ash Resources (Pty) Ltd's ash beneficiation site at Eskom's Lethabo Thermal Power station. This commercial-grade CFA is air-classified on site and is specified to have a mean particle size between 3.9 and 5.0 µm, with more than 90 % of the volume distribution of its particles having a diameter smaller than 11 µm. The CFA sample was sub-divided using a rotary splitter to obtain representative homogeneous sub-samples. Deionised water (analytical grade, electrical conductivity < 1 µS cm^{-1}) was used for all experiments. H_2SO_4 (analytical grade, 98 % w/w) and polyethylene glycol (PEG, 6000) were obtained from Merck (South Africa). The NaOH solution (analytical grade, 50.0 % w/w) and n-butanol (analytical grade) were obtained from Radchem (South Africa).

2.2 Preparation and characterisation of sodium silicate solutions from CFA

CFA was subjected to two distinct leaching processes in order to prepare Na_2SiO_3 solutions of different grades (Figure 1). The first process, hereafter called sequential acid-alkaline leaching (SAAL), is a two-stage process, which involves (i) a H_2SO_4 leaching step for the preferential extraction of Al over Si, followed by (ii) the preferential extraction of Si over Al from the resulting residues using NaOH. The second process is a direct alkaline leaching (DAL) process, which consists of a single-stage elemental extraction from CFA using NaOH, *i.e.* without the preceding acid leaching step used in SAAL. The leaching procedures are discussed in more details below (sections 2.2.1 and 2.2.2). At completion of the leaching experiments, the suspensions were centrifuged to separate the solid and liquid phases. The supernatants were filtered under reduced pressure through 0.4 µm membranes filters (Whatman Nucleopore® Track-Etched polycarbonate, Whatman UK Ltd.) in closed polycarbonate filtration vessels (Sterifil, 47 mm Millipore) and stored at 4 °C. The concentrations of dissolved Al, Si and other elements were determined by ICP-MS at an accredited laboratory (Waterlab Pty Ltd, Pretoria, South Africa). These ICP-MS data were used to calculate elemental extraction efficiencies, *i.e.* the mass fraction of elements extracted from the mass of these elements present in CFA, by comparing them to the XRF data of untreated CFA. The non-dissolved residues were washed thoroughly with deionised water and dried at 80 °C, before being characterised.

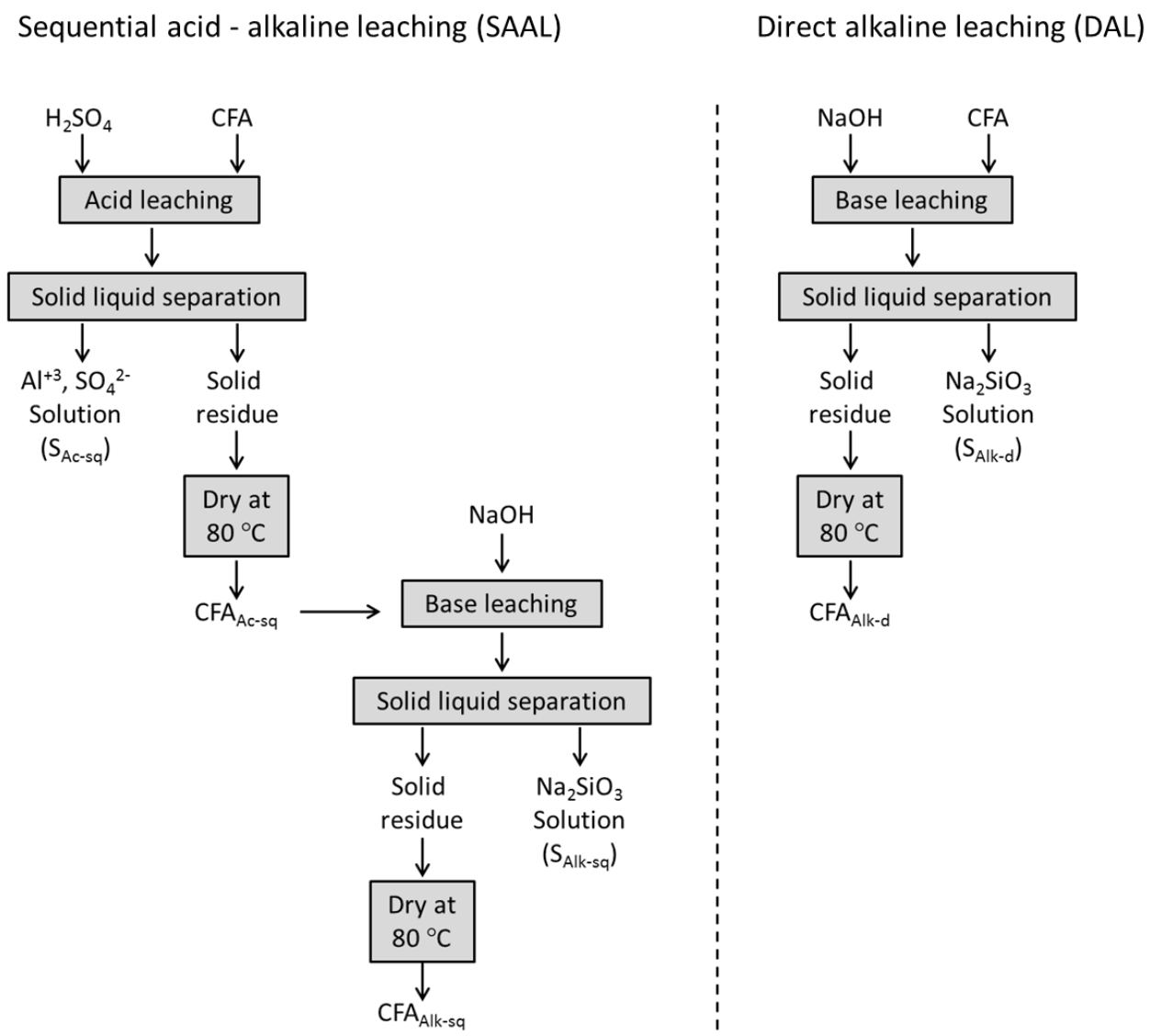

Figure 1. Process flow diagrams for the sequential acid – alkaline leaching (SAAL) and direct alkaline leaching (DAL) extraction of Al, Si and other major elements from CFA.

2.2.1 Sequential acid - alkaline leaching (SAAL)

Step 1 - H_2SO_4 leaching for selective Al extraction

10 g of CFA was dispersed in 100 mL of deionised water (control solutions) or H_2SO_4 of varying concentrations (1; 3; 5; 8 and 10 M; treatment solutions). The suspensions were heated to 95 ± 3 °C in a silicone oil bath, while stirring constantly at 300 rpm using a magnetic stirrer. The reaction mixture was refluxed for different durations ranging between 30 and 480 minutes. The solid residues and supernatants were labelled $CFA_{Ac\text{-}sq}$ and $S_{Ac\text{-}sq}$ respectively (Figure 1).

Step 2 - NaOH leaching for preparation of Na_2SiO_3 solution

The solid residues generated in the first step were dispersed in 100 mL of deionised water (control solutions) or NaOH of varying concentrations (5; 10 and 15 M; treatment solutions). The suspensions were heated in closed high-density polyethylene bottles to 95 ± 3 °C in a silicone oil bath, while stirring constantly at 300 rpm using a magnetic stirrer. The reaction mixture was allowed to react for different durations ranging between 30 and 360 minutes. The solid residues and supernatants were labelled $CFA_{Alk\text{-}sq}$ and $S_{Alk\text{-}sq}$, respectively (Figure 1).

2.2.2 Direct alkaline leaching (DAL)

10 g of CFA was dispersed in a 100 mL solution of 10M NaOH. The suspensions were heated in closed high-density polyethylene bottles to 95 ± 3 °C in a silicone oil bath for 60 minutes, while stirring constantly at 300 rpm using a magnetic stirrer. The NaOH concentration and the reaction duration used were selected since they promoted the highest Si extraction efficiencies in the 2nd step of the SAAL process. The solid residues and supernatants were labelled $CFA_{Alk\text{-}d}$ and $S_{Alk\text{-}d}$ respectively (Figure 1).

2.3 Preparation of silica nanoparticles from sodium silicate solutions

Silica nanoparticles were prepared from the sodium silicate solutions obtained from the SAAL and DAL processes via a sol-gel method. 20 mL of a 3% w/w polyethylene glycol (PEG) solution was sonicated in a 20 Hz ultrasonic water bath at 55 °C for 30 minutes. 80 mL of sodium silicate solution (SAAL or DAL) equilibrated at 55 °C was slowly added to the PEG solution in the ultrasound bath while monitoring the pH of the solution. To initiate the hydrolysis-condensation reaction, 0.5 M H_2SO_4 was gradually added to the sodium silicate solution until a pH of 4 was reached; sonication was continued for another 30 minutes. The resulting gel mixture was aged overnight at 55 °C in a laboratory oven after which the wet-gel silica slurry was separated from the mother liquor by centrifugation. The gel was thoroughly washed with deionised water to remove any remaining Na^+ and SO_4^{2-} ions. A number of successive washing cycles was performed to ensure the removal of SO_4^{2-} ions and $BaCl_2$ was used to test for the presence of SO_4^{2-} ions in the washing water. This was followed by centrifugation and vacuum-filtration. The resulting filtration cake was distilled using 100 mL n-butanol for 2 hours, followed by overnight drying at 120 °C. The resultant powders were subsequently calcined in a

laboratory furnace at 650 °C for 2 hours to remove the remaining PEG and n-butanol. The product masses were recorded to calculate the yield of silica nanoparticles based on the CFA composition and purity of the final silica nanoparticles, using XRF data. The solid products were labelled Si_{SAAL} and Si_{DAL} respectively.

2.4 Characterisation of solid samples

The elemental composition of the solid samples was determined by XRF fused bead analysis (ARL9400XP+ XRF spectrometer, Thermo ARL, Switzerland) while their mineralogy was determined using XRD (PANanalytical X'Pert PRO X-ray diffractometer). Detailed description of these analyses was given elsewhere [28]. A Zeiss Ultra SS (Germany) FESEM, operated at an acceleration voltage of 1 kV, was used under dry high-vacuum condition to observe morphological changes of CFA particles before and after leaching. For this purpose, the powder was mounted on a double-sided carbon tape by dipping carbon stubs into the samples. Excess material was removed by gentle blowing with compressed nitrogen. The sample was sputter-coated with carbon in an Emitech K550X (Ashford, England). A JEOL JEM 2100F TEM was used to study the topography of the silica nanoparticles. The samples were first dispersed in 100% ethanol with the aid of sonication. A drop of the diluted suspension was poured onto a copper grid, which was then placed into the sample injection holder for analysis. Particle size analysis of silica nanoparticles was performed using a Malvern Zetasizer Nano ZS system (Malvern Instruments, Malvern, UK). Approximately 0.01 g of the silica sample was dispersed in 25mL ultra-pure water, and ultrasound was applied at 10% amplitude using an ultrasound probe (Q700 equipped with ¼ inch micro-tip; QSonica, USA) for 1 minute. The sample was equilibrated for 120 seconds prior to particle size measurement. A TriStar II surface area and porosity analyser (Micromeritics, USA) was used with nitrogen gas as adsorbent to determine the bulk surface area by the Brunauer-Emmet-Teller (BET) theory. The samples were degassed at 300 °C for 3 h before performing the gas adsorption tests. FTIR spectra were recorded on a Bruker Alpha Platinum ATR FTIR instrument. Measurements were recorded between 400 to 4000 cm^{-1} at a resolution of 2 cm^{-1}; 64 scans were signal-averaged in each interferogram. Thermogravimetric analyses were performed on a TA Instruments SDT Q600 Thermogravimetric Analyzer (TGA) and Differential Scanning Calorimeter (DSC). Approximately 20 mg of sample was heated from 25 to 1000°C at a heating rate of 20 °C min^{-1} in alumina pans under a dynamic nitrogen atmosphere at a flow rate of 100 mL min^{-1}.

3. Results and discussions

3.1 Characterization of untreated CFA

A detailed surface and bulk characterisation of a similar classified, ultrafine CFA was performed and reported elsewhere [28]. The sample used in this study was obtained from a different batch of this sample and therefore varies slightly in composition; it contains mainly SiO_2 (51.50 wt%), Al_2O_3 (33.60 wt%), CaO (5.18 wt%), Fe_2O_3 (3.40 wt %), TiO_2 (1.89 wt%), MgO (1.02 wt%) and K_2O (1.07 wt%) (Table 1). The mineralogy of CFA consists of an amorphous alumina silica glass phase (64.2 wt%) and two crystalline phases, mullite (28.5 wt%) and quartz (7.2 wt%) respectively (Table 2, Figure 2). Fly ash particles are predominantly spherical in shape with a relatively smooth surface texture and their sizes vary from sub-microns up to *ca.* 10 µm (Figure 3, top micrograph; and Figures 3 and 4 in van der Merwe *et al.* [28]).

Table 1. Chemical composition of untreated CFA and solid residues following the acid leaching step of the SAAL process ($CFA_{Ac\text{-}sq}$, obtained from 5 M H_2SO_4 over 240 min), alkaline leaching step of the SAAL process ($CFA_{Alk\text{-}sq}$), and alkaline leaching step of the DAL process ($CFA_{Alk\text{-}d}$). ($CFA_{Alk\text{-}sq}$ and $CFA_{Alk\text{-}d}$ both obtained from 10 M NaOH over 60 min).

	Concentration (wt. %)			
Composition	CFA	$CFA_{Ac\text{-}sq}$	$CFA_{Alk\text{-}sq}$	$CFA_{Alk\text{-}d}$
SiO_2	51.50	45.15	36.60	32.50
Al_2O_3	33.60	24.20	36.70	30.80
CaO	5.18	2.57	2.93	5.20
Fe_2O_3	3.40	1.37	2.11	2.80
TiO_2	1.89	1.12	1.81	1.74
K_2O	1.07	0.78	0.27	0.21
MgO	1.02	0.44	0.66	1.10
P_2O_5	0.70	0.10	0.06	0.24
SO_3	0.44	0.46	0.13	0.14
Na_2O	0.16	0.18	9.68	14.00
LOI	0.92	23.4	7.33	10.40

Total	99.88	99.77	98.28	99.13
SiO_2/Al_2O_3 ratio	1.5	1.9	1.0	1.1
Si/Al ratio	1.4	1.7	0.9	0.9

Table 2. Mineralogical composition of untreated CFA and the solid residues following the acid leaching step of the SAAL process ($CFA_{Ac\text{-}sq}$), alkaline leaching step of the SAAL process ($CFA_{Alk\text{-}sq}$), and alkaline leaching step of the DAL process ($CFA_{Alk\text{-}d}$). Experimental conditions given Table 1.

Mineral/Phase	Chemical composition	Abundance (wt. %)			
			SAAL process		DAL process
		CFA	$CFA_{Ac\text{-}sq}$	$CFA_{Alk\text{-}sq}$	$CFA_{Alk\text{-}d}$
Amorphous	-	64.2	59.8	39.5	70.3
Mullite	$Al_6Si_2O_{13}$	28.5	28.0	44.3	14.7
Quartz	SiO_2	7.2	7.6	9.5	2.7
Anhydrite	$CaSO_4$	-	4.5	-	-
Hydrosodalite	$Na_8[AlSiO_4]_6(OH)_2{\cdot}nH_2O$	-	-	6.8	12.3

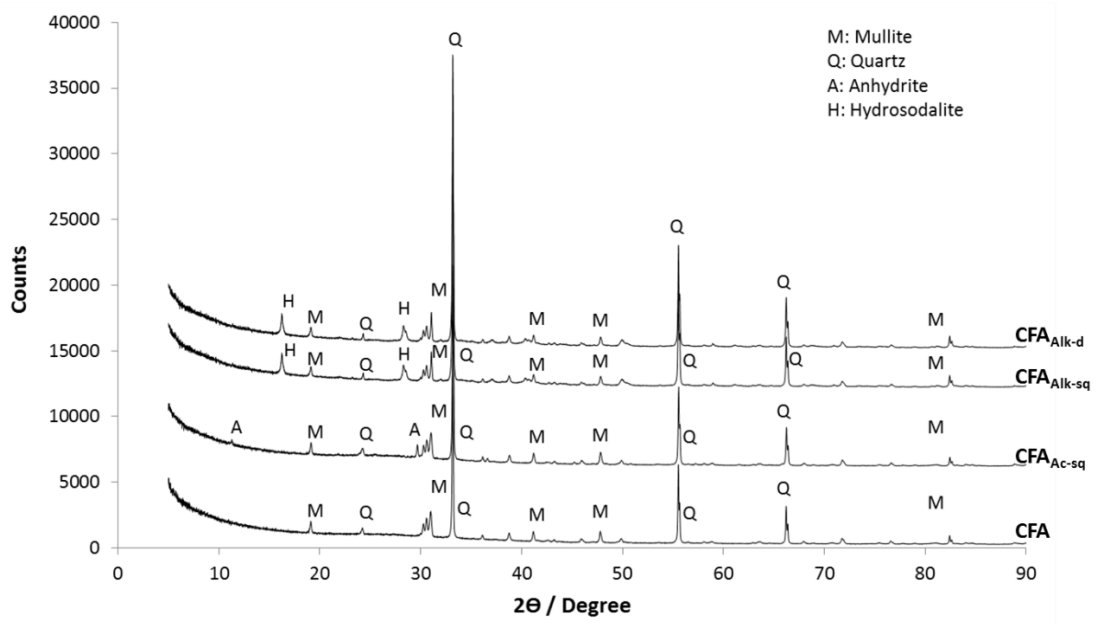

Figure 2. XRD analysis of untreated CFA, $CFAA_{c\text{-}sq}$, $CFA_{Alk\text{-}sq}$ and $CFA_{Alk\text{-}d}$.

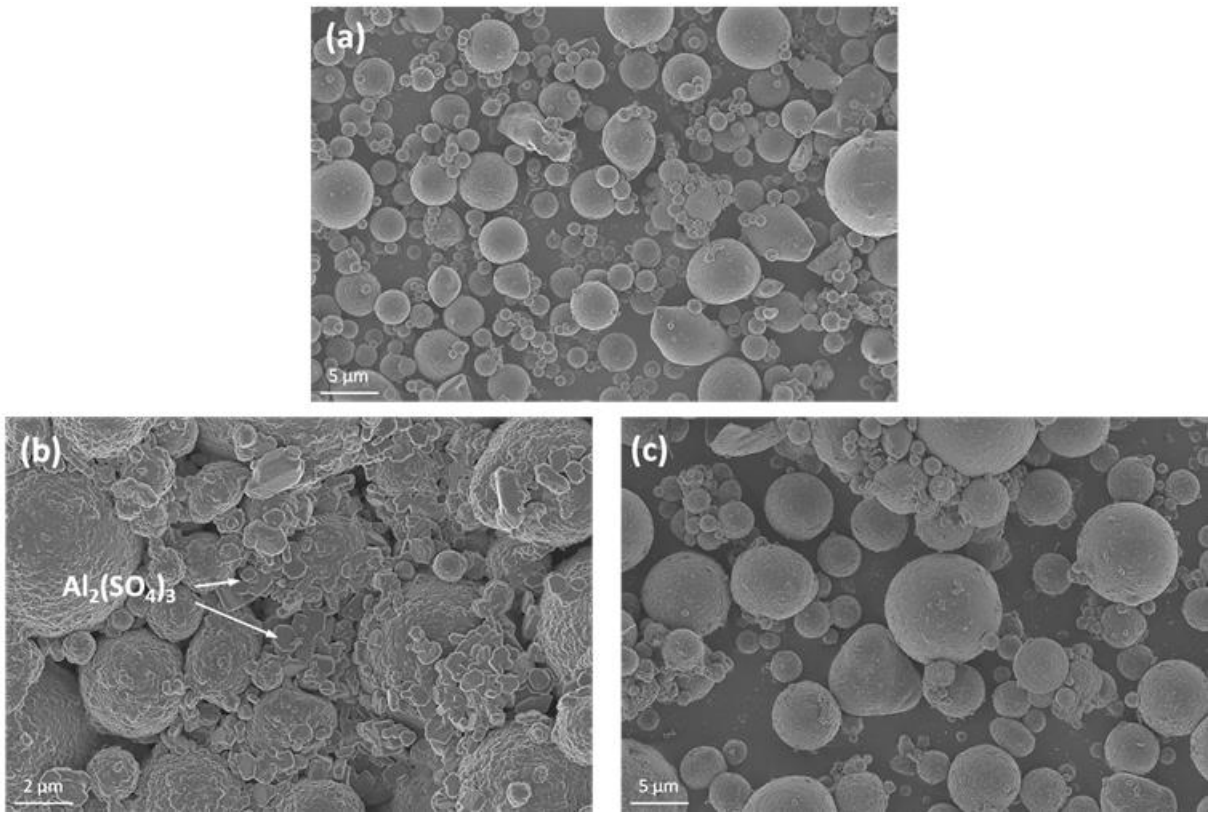

Figure 3. FESEM images of (a) CFA, (b) unwashed $CFA_{Ac\text{-}sq}$ and (c) $CFA_{Ac\text{-}sq}$ washed with water.

3.2 Sequential acid - alkaline leaching (SAAL) process

3.2.1 Acid leaching step

Extraction of Si and Al from CFA may occur from the amorphous alumina silica glass phase and/or the crystalline phases (*i.e.* mullite and quartz). It was anticipated that extraction of Si and Al from the crystalline phases would be minimal. For this reason, elemental extraction efficiencies were calculated and presented both as percentage extracted from the amorphous phase, and as a percentage of the total Al and Si present in CFA, as done in our previous study [29]. The total content of Al in CFA, expressed as Al_2O_3, was 33.6 wt%, which corresponds to 17.8 g Al/100 g CFA. The speciation of Al in CFA was two-fold: it occurs in the crystalline phase as mullite (CFA contains 28.5 wt% mullite, which is theoretically composed of 38 wt% Al), while the remainder of the total Al is contained in the amorphous glass phase. This implied that 10.9 g of the total 17.8 g Al/100g CFA was confined in the potentially unreactive mullite fraction, while the remaining 6.9 g of Al occurred in the more reactive amorphous glass phase. Similar calculations for the extraction of Si indicated that 16.9 g of Si was contained in the amorphous phase, with the residual 7.1 g trapped in the less reactive silicon-containing crystalline phases (*i.e.* mullite and quartz).

Figures 4(a) and (b) show the results of the extraction efficiency of Si and Al from CFA as a function of reaction time for leaching experiments performed using various concentrations of H_2SO_4. This acid leaching step was performed to attempt maximum removal of reactive Al and other impurities from CFA, with minimum loss of Si. A low H_2SO_4 concentration (1 M) caused the rapid co-extraction of Al and Si (37% and 11% from the amorphous phase respectively) within 30 min, with no improvement with increased leaching time. Co-extraction of Si and Al from South African coal fly ash in dilute aqueous solutions of H_2SO_4 was already reported elsewhere [30]. Using H_2SO_4 concentrations of 3 M and above was successful in minimising Si loss (< 0.6% total Si). The low extraction efficiency of Si at increased H_2SO_4 concentrations can be attributed to silica gel formation, leading to low solubility of Si under strong acidic conditions (i.e. very low pH). Verbaan and Louw [30] reported a reduction in Si extraction from CFA into aqueous solutions containing high concentrations of H_2SO_4, due to silica gel formation.

Increasing the H_2SO_4 concentration up to 5 M enhanced Al extraction up to 82% from the amorphous phase (32% total Al), whereas 8 M and 10 M H_2SO_4 solutions caused lower Al extraction (17-26% from amorphous phase, 7-10% total Al). The best extraction of Al was obtained using 5 M H_2SO_4 for all leaching times studied (Figures 4(a) and (b)). Increasing the reaction time from 120 to 240 min resulted in a substantial improvement in Al extraction (57 to 82% from the amorphous phase) when using 5 M H_2SO_4; this was not observed in experiments using other concentrations of H_2SO_4. This prompted further experiments with 5 M H_2SO_4 that showed lower Al extraction efficiencies with longer leaching durations (Figures 4(c) and (d)). Reduction in Al extraction was explained by the secondary precipitation of aluminium sulphate ($Al_2(SO_4)_3$) with and without the oxonium ion in its structure(Figure S1). The occurrence of anhydrite ($CaSO_4$) was also observed. The presence of $Al_2(SO_4)_3$-phases was further confirmed by FESEM observation (Figure 3(c)) of particles having their typical hexagonal plate-like habit [29,31]. These particles are highly water-soluble and were not observed in the FESEM micrographs (Figure 3(b)) and XRD spectra (Figure 2, Table 2) of washed solid residues. Elucidation of their mechanism of precipitation falls outside the scope of this paper, although it is most likely that these phases would have occurred via direct precipitation in solution, or via precipitation at the surface of the fly ash particles. The latter mechanism was observed during acid dissolution of Al from waste aluminium dross, a waste residue remaining after the melting of aluminium in the presence of air [32].

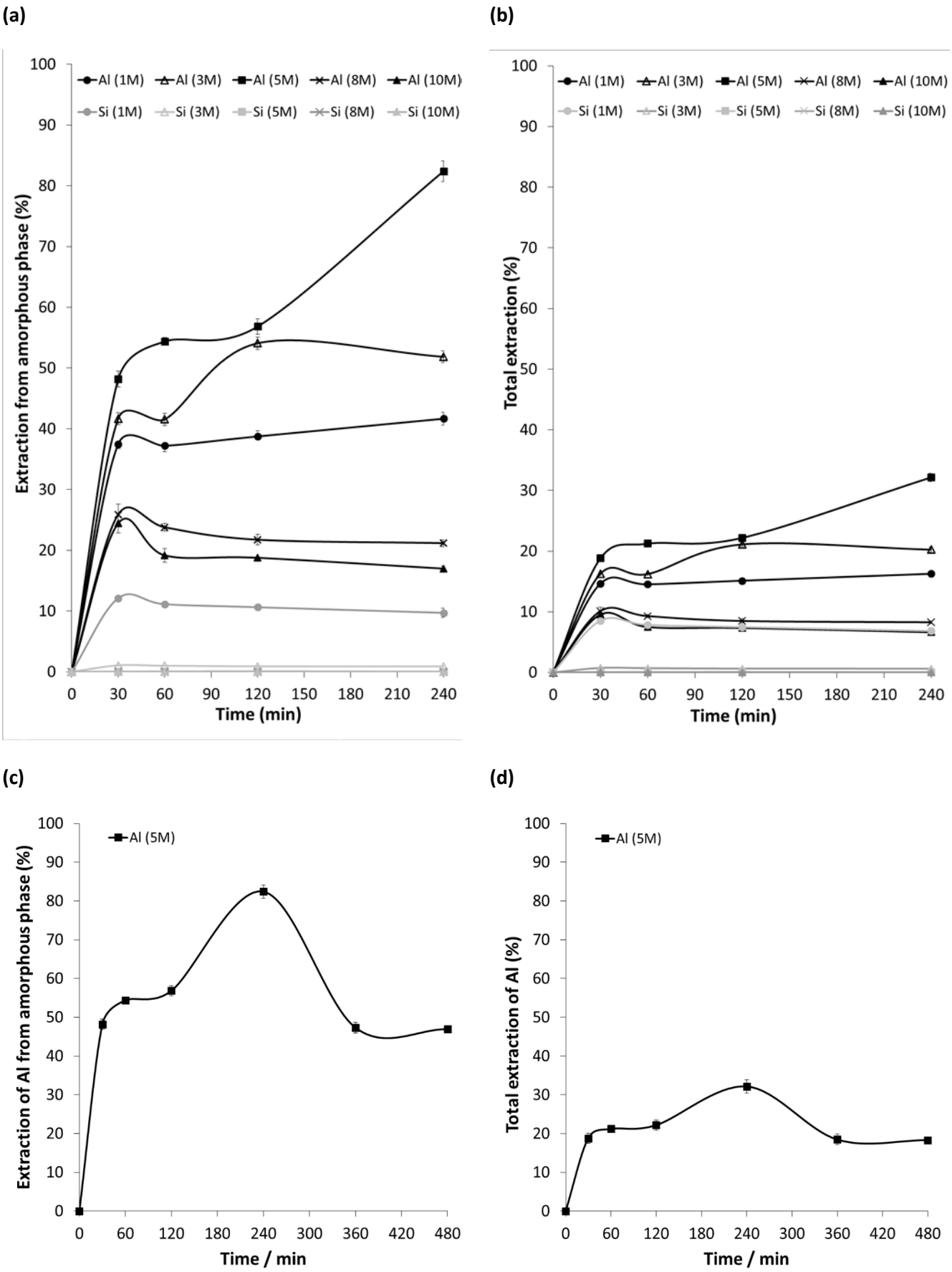

Figure 4. Effect of leaching time and H_2SO_4 concentration on (a) Si and Al extraction efficiency from the CFA amorphous phase and (b) corresponding total Si and Al extraction from CFA; and the effect of increasing the leaching time in 5 M H_2SO_4 on (c) Al extraction from the amorphous phase and (d) total Al extraction from CFA. Concentrations in the legend refer to H_2SO_4 concentration (*n = 3*).

In brief, the most favourable conditions for the extraction of the most reactive phases of Al (82% from the amorphous phase, 32% total) with minimal loss of Si (< 0.6% total) during the acid leaching step of the SAAL process were 5 M H_2SO_4 and a leaching time of 240 min at 95 °C. This extraction efficiency is comparable to the results obtained previously on the same CFA sample [29,33] where total Al extraction efficiencies between 30.5 – 37.3% were obtained via thermochemical treatment of CFA with ammonium sulphate and ammonium bisulphate followed by aqueous leaching. It was also similar to that achieved (85% from the amorphous phase) on unclassified South African CFA via direct leaching in 6 M H_2SO_4 at 75 °C over a period of 8 h 45 min [34]. Comparison of our results to that of Shemi et al. [34] indicate that similar Al extraction efficiencies may be reached upon decreasing the temperature of the acid leaching step (95 °C *vs* 75 °C) and increasing the leaching time (6 h *vs* 8 h 45 min) at a H_2SO_4 concentration between 5 - 6 M.

3.2.2 Alkaline leaching step

The Si-enriched solid residue ($CFA_{Ac\text{-}sq}$; Figure 1) obtained from the acid leaching step (Section 3.2.1) was used as starting material for the preparation of sodium silicate (Na_2SiO_3) solutions via leaching in NaOH solution during the alkaline leaching step. The chemical and mineralogical compositions of $CFA_{Ac\text{-}sq}$ are reported in Tables 1 and 2 respectively. Figure 5 shows the results of the total extraction efficiency of Si and Al from $CFA_{Ac\text{-}sq}$ as a function of reaction time, for leaching experiments performed at 95 °C using various concentrations of NaOH. The purpose of this alkaline leaching step was to achieve maximum extraction of Si with minimum co-extraction of Al and other contaminants.

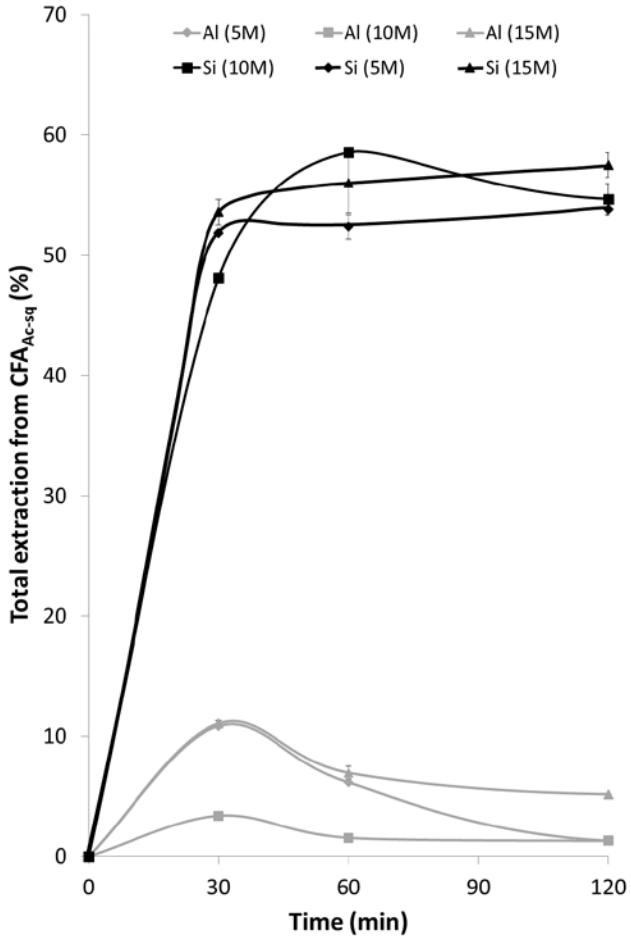

Figure 5. Effect of leaching time and NaOH concentration on Si and Al extraction efficiency from CFA_{Ac-sq}. Concentrations in the legend refer to NaOH concentration (*n = 3*).

Rapid co-extraction of Si and Al was observed under all alkaline conditions, with the highest amount (*ca*. 9.2%) of extracted Al measured after 30 min of leaching (Figure 5). This was followed by a decrease in dissolved Al over time, with the lowest percentage of total Al (*ca.* 1.6%) being obtained after 60 min of leaching in 10 M NaOH or after 120 min in 5 M NaOH. The lowering in dissolved Al concentration was most probably due to secondary mineral precipitation, for instance of zeolite crystallites in the form of hydrosodalite ($Na_8(AlSiO_4)_6(OH)_2.nH_2O$) as identified by XRD (Figure 2), although it was not observed during FESEM imaging (Figure 6(a)). This mineral represented as much as 6.8 wt% of CFA_{Alk-sq} produced from leaching CFA_{Ac-sq} in 10 M NaOH for 1 hour at 95°C (Table 2), which can only partially explain the lowering of dissolved Al. Its occurrence explained the increase in the content of Na_2O from 0.16 wt% in untreated CFA to 9.68 wt% in CFA_{Alk-sq} following treatment (Table 1). The formation of hydrosodalite during NaOH leaching of coal fly ash was previously documented [35,36]. Other types of zeolite minerals (such as analcime [36] and herschelite [37]) were also reported.

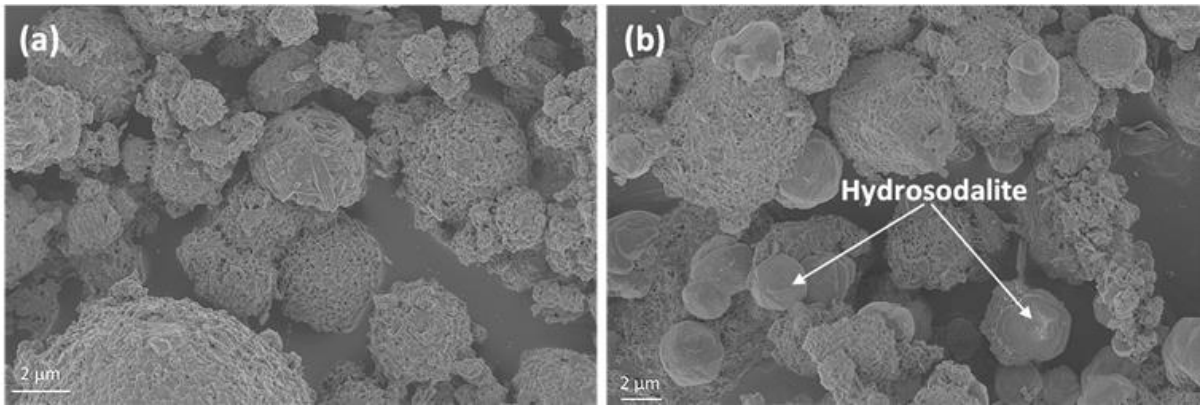

Figure 6. FESEM images of (a) $CFA_{Alk\text{-}sq}$, and (b) $CFA_{Alk\text{-}d}$.

FESEM was useful in illustrating changes in the surface topography of CFA particles, from smooth surfaces in untreated CFA (Figure 3(a)) to the presence of small pores at the surface of $CFA_{Alk\text{-}sq}$ residues after leaching in NaOH (Figure 6(a)). This suggested substantial dissolution of Si from the amorphous $CFA_{Ac\text{-}sq}$ surface under alkaline conditions. This was confirmed by ICP analysis of leachates, which showed that up to 89% of Si had been extracted from the amorphous phase of $CFA_{Ac\text{-}sq}$ (corresponding to a total extraction efficiency of 59%; Figure 5) for leaching performed in 10 M NaOH over 60 minutes. These values correspond to extraction efficiencies of 61% of Si from the amorphous phase of the original CFA sample, or a total extraction efficiency of 42%. XRF analysis of the solid residues (Table 1) further confirmed extensive Si removal from $CFA_{Ac\text{-}sq}$, with its SiO_2/Al_2O_3 ratio of 1.9 being higher than that of $CFA_{Alk\text{-}sq}$ (SiO_2/Al_2O_3 ratio of 1.0). These conditions also corresponded to the minimal Al extraction reported earlier (*ca.* 1.6%). Lowering the NaOH concentration to 5 M had a negative effect on Si extraction efficiency from $CFA_{Ac\text{-}sq}$ (80% from amorphous phase, i.e. 53% total; Figure 5). Extensive extraction of Si from the amorphous aluminosilicate glass phase contained in CFA under alkaline leaching conditions, and low extraction from the crystalline mullite and quartz phases, have been widely reported (e.g. [38]). XRD confirmed a lower proportion (39.5%) of amorphous material in $CFA_{Alk\text{-}sq}$ than in the starting material $CFA_{Ac\text{-}sq}$ (59.8%; Table 2), which was in agreement with the dissolution of the amorphous phase.

In brief, the most favourable conditions for Si extraction from $CFA_{Ac\text{-}sq}$ (89% from the amorphous phase, 59% total) with minimal loss of Al (< 2% total) during the alkaline leaching step of the SAAL process were 10 M NaOH and a leaching time of 60 minutes at 95 °C.

3.3 Direct alkaline leaching (DAL)

In this process, simultaneous co-extraction of Al and Si was evaluated under direct alkaline leaching condition, *i.e.* in the absence of a preceding acid leaching step. The experiments were performed using the optimal experimental conditions obtained for the alkaline leaching step of the SAAL process (*i.e.* 10 g CFA / 100 mL NaOH 10 M at 95 °C for 1 hour). Substantial extraction of Si (60.4 % from amorphous phase, 42.4 % total) was achieved under these conditions, with as much as 16.6% from amorphous phase or 6.4% from the total content of Al extracted. These results were reflected in the change in SiO_2/Al_2O_3 ratio between untreated CFA (1.5) and the solid residue $CFA_{Alk\text{-}d}$ (1.1) (Table 1). These results are comparable to that of Sedres [39] who reported total extraction efficiencies of 48 % for Si and 3% for Al under alkaline leaching of CFA using 6.25 M NaOH at 100^{o}C for 2 hours.

The formation of hydrosodalite in $CFA_{Alk\text{-}d}$ (Figure 2) was observed in greater proportion (12.3 wt%; Table 2) than in the solid residue $CFA_{Alk\text{-}sq}$ (6.8 wt%) obtained from the SAAL process. Its occurrence explains the Na_2O content of 14.0 wt% in $CFA_{Alk\text{-}d}$ (Table 1) and was confirmed by direct observation using FESEM (Figure 6(b)), which showed its characteristic morphological features as spherical structures with protruding surfaces [36]. The formation of zeolite during Si extraction was not a limiting factor in the extent of Si that could be recovered, as alluded in other studies [37], since in the present work 12.3 wt% hydrosodalite would only account for <1% of the total Si contained in untreated CFA.

3.4 Extraction of major elements from CFA during SAAL and DAL

Extraction efficiencies of major elements from CFA using the two processes are summarised in Figure 7. Similar extraction efficiencies for Si (42%) were achieved for the two processes, but the SAAL process provided the added advantage of selectively extracting Al and Si in two distinct processing stages, which resulted in minimising their co-extraction. In particular, < 2% of Al was extracted during the Si extraction step (alkaline leaching) of the SAAL process, compared to 6% obtained with the DAL process.

In addition, the inclusion of the acid leaching step in the SAAL process assisted with the substantial extraction of other major elements (> 48% for Fe and Ti; > 88% for Mg), with minimal loss of Si (< 0.6% total). Ca extraction, which was calculated from ICP analysis of leachates, appeared low (2.5%), but the result is misleading. XRD demonstrated the formation of anhydrite ($CaSO_4$, 4.5 wt%; Table 2) via secondary precipitation, which led to lower Ca concentrations in solution. The secondary precipitate

represents approximately 30% of the total Ca contained in untreated CFA. This Ca extraction efficiency was low compared to those previously achieved for a similar South African CFA sample using thermochemical treatment with ammonium sulphate (57%; [29]), or ammonium bisulphate and mixtures of these two ammonium-based reagents (45%; [33]).

The acid leaching step of the SAAL process could arguably be replaced by thermochemical treatment of CFA with ammonium sulphate followed by aqueous dissolution at 25°C. The latter was shown to achieve similar co-extraction of reactive Al (31%), and reasonable but lower extraction of other major elements, with < 0.6% of extracted Si [29].

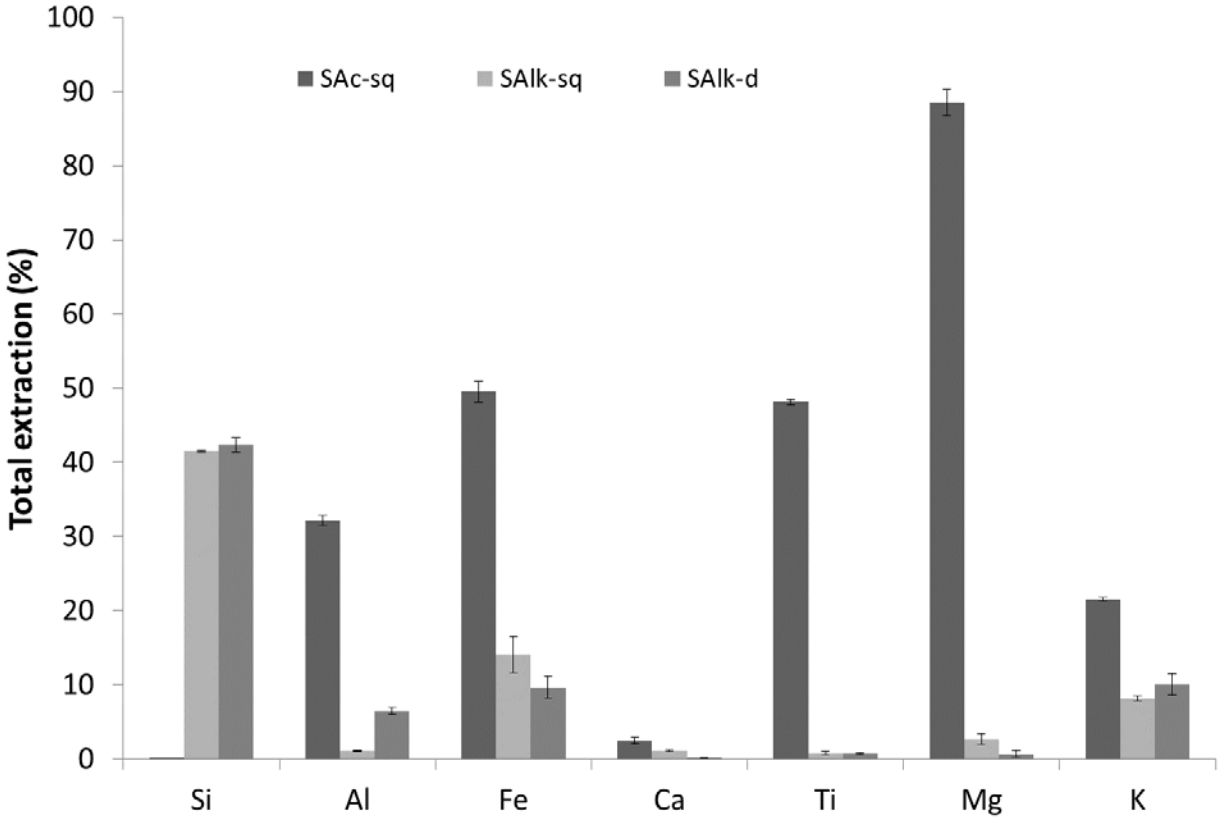

Figure 7. Summary of extraction efficiency of the main elements from CFA using the sequential acid – alkaline leaching (SAAL) vs direct alkaline leaching (DAL) extraction processes *(n = 3)*.

Table 3. Elemental composition (mg/L) of the sodium silicate solution following sequential acid - alkaline leaching (S_{Alk-sq}) and direct alkaline leaching (S_{Alk-d}) *(n = 3)*.

	Al	As	Au	B	Ba	Be	Ca	Co	Cr	Cs
S_{Alk-sq}	166.39	0.17	0.08	2.89	1.68	0.13	29.42	0.09	0.09	0.93
Std Dev	6.98	0.08	0.04	1.07	0.13	0.02	11.90	0.01	0.08	0.36
S_{Alk-d}	1158.33	0.64	0.02	2.67	4.40	0.15	7.19	0.24	0.17	1.39
Std Dev	94.19	0.09	<0.01	0.49	2.12	0.05	1.45	0.08	0.06	0.31

	Cu	Fe	Ga	Ge	Hf	In	K	Li	Mg	Mn
S_{Alk-sq}	0.25	158.00	2.43	1.12	0.04	<0.01	806.23	15.72	8.24	3.86
Std Dev	0.27	27.35	0.84	0.46	0.02	0.00	312.49	2.79	2.29	0.65
S_{Alk-d}	<0.01	231.73	5.18	0.45	0.06	0.02	901.30	16.59	3.79	5.57
Std Dev	<0.01	35.27	1.26	0.10	0.01	0.01	124.71	3.75	2.47	0.96

	Mo	Na	Nb	Ni	P	Pb	Rb	Sb	Sc	Se
S_{Alk-sq}	0.11	188750.00	0.02	0.97	44.35	2.10	5.53	0.21	0.03	0.59
Std Dev	0.04	2757.72	0.00	0.06	15.07	1.10	2.37	0.06	0.01	0.52
S_{Alk-d}	0.41	187833.33	0.02	0.60	96.30	7.92	8.39	0.11	0.11	0.38
Std Dev	0.06	5558.18	0.01	0.01	17.08	2.85	1.80	0.03	0.01	0.04

	Si	Sn	Sr	Ti	Tl	U	V	W	Zn	Zr
S_{Alk-sq}	10261.57	1.01	0.10	6.08	0.01	0.12	4.49	0.34	2.92	0.47
Std Dev	33.54	0.39	0.02	1.71	0.00	0.11	1.91	0.13	0.57	0.13
S_{Alk-d}	10320.00	1.42	0.40	7.78	<0.01	0.14	19.43	0.72	3.10	1.26
Std Dev	173.21	0.24	0.16	1.51	<0.01	0.01	3.10	0.08	0.66	0.16

3.5 Chemical composition and pH of sodium silicate solutions obtained from SAAL and DAL

The chemical compositions of Na_2SiO_3 solutions obtained from the two processes are summarised in Table 3. The purpose of studying the two processes was to yield Na_2SiO_3 solutions containing low concentrations of Al and other contaminants, as precursor for silica nanoparticle synthesis. The pH of the two Na_2SiO_3solutions was identical (i.e. 11.8). They exhibited similar Si content (10.2-10.3 g/L), but their Al content differed greatly. Inclusion of the acid leaching step in the SAAL process yielded a sodium silicate solution with significantly lower Al content (166 mg/L *vs* 1158 mg/L). Similar amounts of Fe (± 200 mg/L) and K (± 800 mg/L) were measured as impurities in the two solutions. The amount of Ca (29 mg/L *vs* 7 mg/L) was higher in Na_2SiO_3 obtained from SAAL.

3.6 Characterisation of silica nanoparticles obtained from sodium silicate solutions

Silica nanoparticles prepared from SAAL and DAL sodium silicate solutions via the sol-gel method were characterised in terms of chemical (Table 4) and mineralogical (Figure 8) compositions, and structural and textural properties (Figure 9, Table 5). All samples of synthesised silica nanoparticles were characterised by a high level of purity (96.3 - 98.6 wt% SiO_2), with most of the deviation from 100% being due to moisture as a result of the hygroscopic nature of the samples, as confirmed by TGA (Figure S2). Conversion of the XRF data to a dry weight basis indicated that the actual purity of the synthesised silica nanoparticles ranged between 98.8 – 99.3%. The product obtained from the DAL process contained a marginally greater amount of Al_2O_3 (0.45 wt%) than that from SAAL (0.13 wt%), while the CaO (0.2 - 0.3 wt%), MgO (0.1-0.2 wt%) and Na_2O (<0.1 wt%) content of the products were similar. Very low amounts (<0.03 wt%) of Fe_2O_3, TiO_2, K_2O, P_2O_5 and SO_3 were observed (Table 4). The content of these impurities accounted for about 0.68 wt%, and indicated that the synthesis process requires further optimisation in order to prevent their undesired inclusion and therefore to yield ultra-pure Si nanoparticles (i.e. ≥ 99.9 wt% SiO_2). The presence of the broad band centred at 2θ=22.5° and the absence of sharp peaks in the XRD spectra (Figure 8) confirmed the amorphous nature of the silica nanoparticles [14]. FTIR spectra (Figure S3) displayed characteristic peaks related to Si−O-Si vibrational modes detected around 460 cm^{-1} (Si-O rocking), 800 cm^{-1} (Si-O bending) and 1070 cm^{-1} (Si−O−Si asymmetric stretching) which are typical of silica nanoparticles [40,41]. The disappearance of the additional peaks between 520-1800 cm^{-1} for Si_{SAAL} and Si_{DAL} following calcination indicated the effectiveness of the calcination process in removing n-butanol and PEG used during the synthesis. This result was confirmed by TGA analysis of the samples before and after calcination (Figure S2).

Dehydration of the silica nanoparticles, and decomposition and oxidation of PEG and n-butanol, was evident from the high mass loss (*ca.* 35 wt%) observed up to 600°C [23]. After calcination, Si_{SAAL} and Si_{DAL} exhibited a low mass loss (< 3 wt%), which was ascribed to the loss of absorbed surface water, over the same temperature range.

FESEM and TEM illustrated that primary silica nanoparticles were approximately spherical with sizes ≤ 200 nm and had aggregated to form micron-size agglomerates (Figure 9). Although the samples appeared monomodal when analysed by dynamic light scattering (DLS) (data not reported), the technique provided limited information on the size of primary nanoparticles since the polydispersity index (PDI) was greater than 0.1, ranging between 0.4 and 0.7. Since FESEM and TEM indicated limited polydispersity, the high value of PDI was likely due to particle aggregation which could not be prevented by ultrasound.

Textural parameters (Table 5) of Si_{SAAL} and Si_{DAL} indicated surface areas exceeding 500 $m^2\ g^{-1}$, pore volumes around 0.4 $cm^3\ g^{-1}$ and average pore diameters in the range of 2.5 nm. According to IUPAC classification, the prepared silica powders can be classified as mesoporous materials, for which pore size is in the range of 2–50 nm [42].

Table 4. Chemical composition (wt. %) of silica nanoparticles obtained from the sodium silicate solutions prepared via the SAAL and DAL processes.

	SiO_2	Al_2O_3	CaO	MgO	Na_2O	Fe_2O_3	TiO_2	K_2O	P_2O_5	SO_3	Total
Si_{SAAL}	98.62	0.13	0.21	0.16	0.08	0.01	0.02	0.03	0.02	0.02	99.3
Si_{DAL}	96.30	0.45	0.33	0.21	0.08	0.02	0.02	0.03	0.02	0.02	97.5

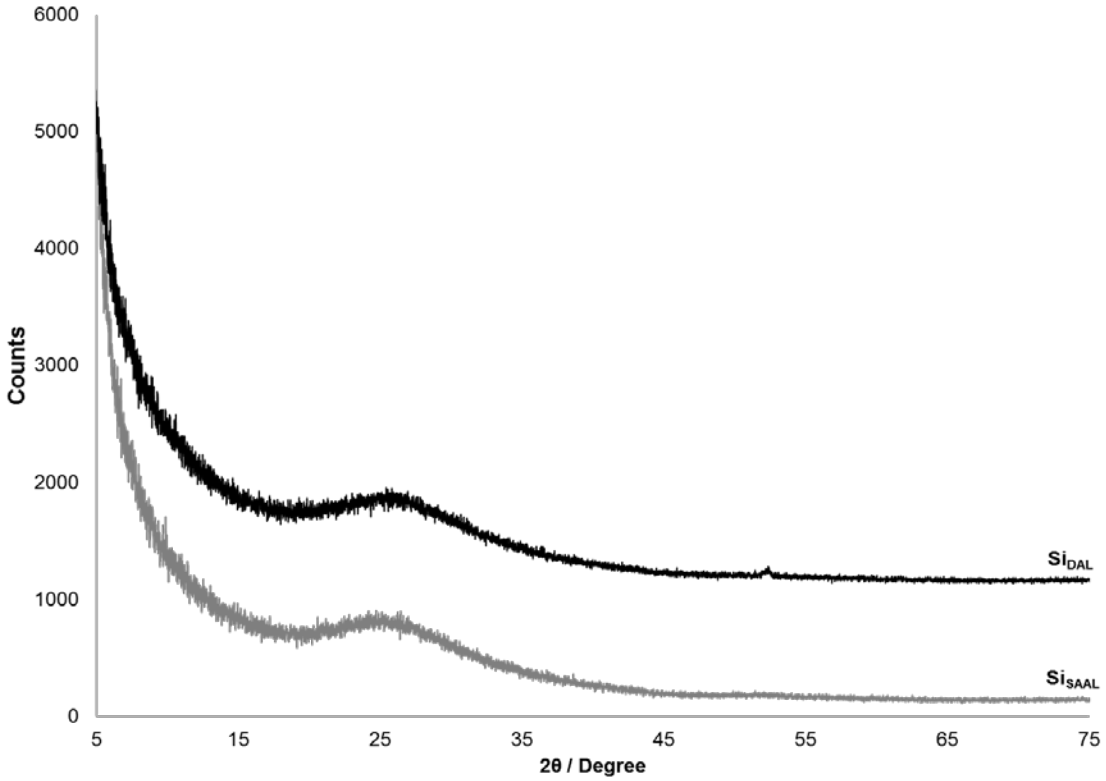

Figure 8. XRD analysis of silica nanoparticles, Si_{SAAL} and Si_{DAL}, obtained from fly ash derived sodium silicate **solutions.**

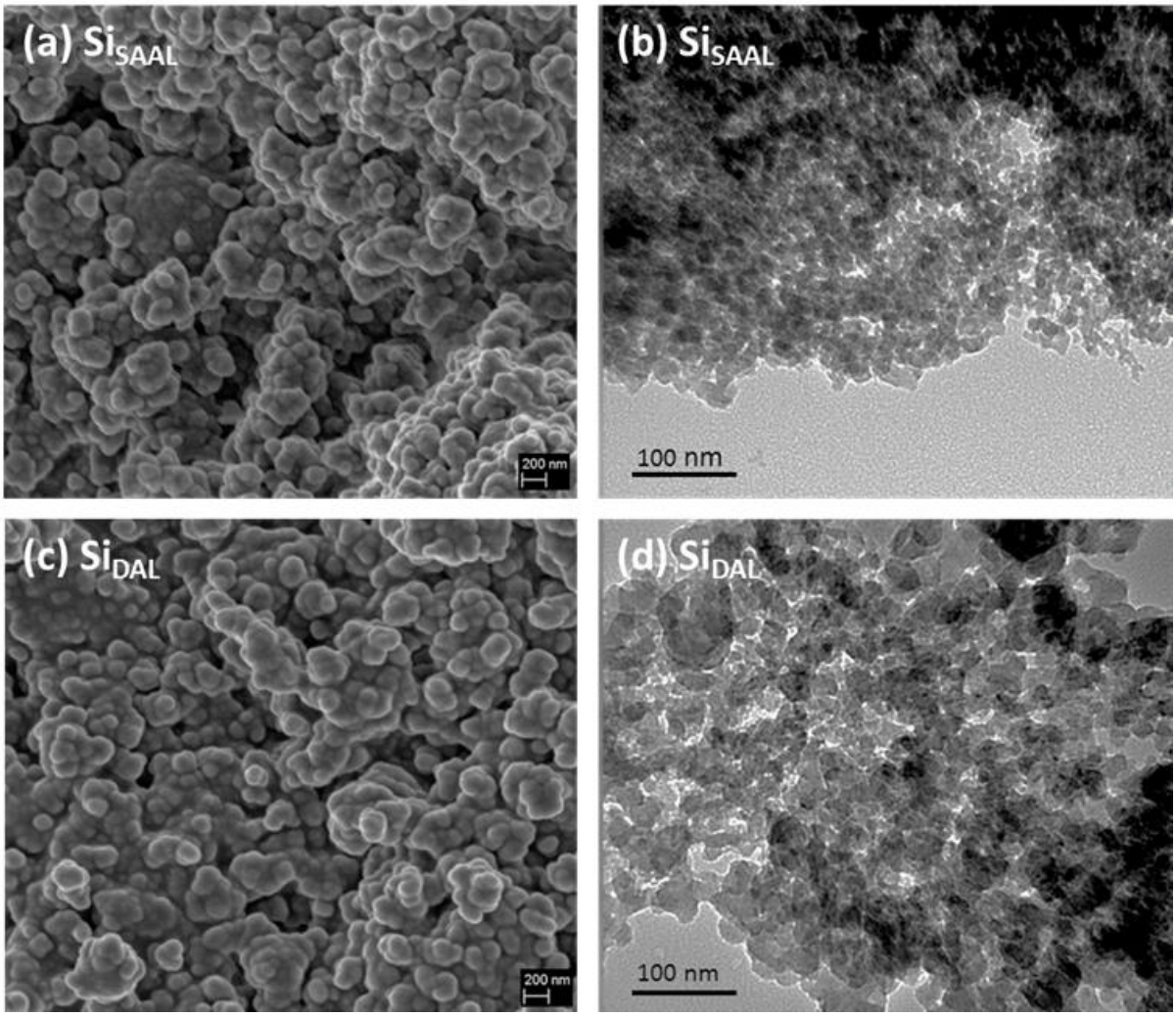

Figure 9. FESEM (a, c) and TEM (b, d) images of silica nanoparticles prepared from SAAL (a, b) and DAL (c, d) sodium silicate solutions.

Table 5. Textural parameters and average particle size of the silica particles obtained from the sodium silicate solutions prepared via the SAAL and DAL processes.

	BET surface area ($m^2\ g^{-1}$)	Average pore diameter (nm)	Pore volume ($cm^3\ g^{-1}$)	Average particle size (nm; FE-SEM and TEM data)
Si_{SAAL}	515.3	2.74	0.353	≤ 200 nm
Si_{DAL}	651.2	2.52	0.411	≤ 200 nm

3.7 Estimated economic feasibility

On the basis of our laboratory studies, the synthesis of amorphous mesoporous silica nanoparticles from South African coal fly ash waste is feasible and economically promising. The treatment of 1 ton

of ash yields about 0.155 ton of nano-SiO_2. This volume could be valued at R607 million if optimal specifications are achieved; *e.g.* based on the price of nano-SiO_2 taken as R3 920 per gram for mesoporous silica nanoparticles with mean particle size of 190-250 nm and pore size of 3.5-4.5 nm sold by Sigma-Aldrich [43]. This compares favourably with the input costs of the main raw materials: coal fly ash and the reagents. The cost of the commercial-grade coal fly ash used in this study is R161/t. The transport cost of ash is site-specific and cannot be estimated for the process. It was therefore not taken into account, although it is most likely to represent the bulk of the input costs related to the main raw materials. The process leads to the generation of approximately 740 kg of solid residue per ton of processed ash. The residue is characterised by a Si:Al of 0.9 (Table 1), which may be suitable as starting material for the preparation of geopolymer bricks or ceramics with a strong, rigid 3D aluminosilicate network [44], or of other lightweight construction materials [45]. The former application is currently being tested in the authors' laboratories and if successful, could demonstrate the concept of circular economy in the context of the South African electricity generation landscape. Another major advantage of the process of conversion of coal fly ash to commercial-grade products lies in the savings on ash waste disposal costs. Long-term storage and management of ash waste dumps present economic as well as potential environmental challenges. Not only are these dumps unsightly, but they also occupy large areas of land and require long-term expenditures for maintenance and monitoring.

4. Conclusions

Two processes for the preparation of Na_2SiO_3 solutions and the subsequent synthesis of silica nanoparticle from coal fly ash waste were studied. During the sequential acid-alkaline leaching (SAAL) process, preferential extraction of reactive Al over Si was achieved via H_2SO_4 leaching, while preferential extraction of Si over Al occurred from the resulting residues using NaOH. In comparison, the direct alkaline leaching (DAL) process consisted of a single-stage elemental extraction from fly ash using NaOH. The two extraction processes generated Na_2SiO_3 solutions with identical pH (11.8), similar Si (10.2-10.3 g/L), Fe (*ca.* 200 mg/L) and K (*ca.* 800 mg/L) content, and low Ca and Mg concentrations (≤ 29 mg/L). Selective extraction of Al and Si was achieved by the SAAL process, resulting in a Na_2SiO_3 solution with significantly lower Al content (166 mg/L *vs* 1158 mg/L).

Sub-200 nm amorphous mesoporous silica nanoparticles can be successfully produced from sodium silicate precursors extracted from South African coal fly ash via either sequential acid - alkaline leaching or direct alkaline leaching processes. The SAAL process is preferred when production of high-

purity of silica nanoparticles (> 99 wt% SiO_2) is required, whereas the more affordable DAL process can be used for applications where silica nanoparticles of lower purity are suitable. Produced nanoparticles are currently being tested for catalyst support applications.

References

1. Reynolds-Clausen, K., Singh, N.: Eskom's revised Coal Ash Strategy and Implementation Progress, in: In Proceedings of World of Coal Ash (WOCA) Conference, Lexington, Kentucky, USA, 2017. www.flyash.info

2. Naik, S.P., Sokolov, I.: Room temperature synthesis of nanoporous silica spheres and their formation mechanism. Solid State Commun. 144, 437–440 (2007). doi:https://doi.org/10.1016/j.ssc.2007.09.033

3. Venkateswara Rao, A., Hegde, N.D., Hirashima, H.: Absorption and desorption of organic liquids in elastic superhydrophobic silica aerogels. J. Colloid Interface Sci. 305, 124–132 (2007). doi:https://doi.org/10.1016/j.jcis.2006.09.025

4. Yang, M., Wang, G., Yang, Z.: Synthesis of hollow spheres with mesoporous silica nanoparticles shell. Mater. Chem. Phys. 111, 5–8 (2008). doi:https://doi.org/10.1016/j.matchemphys.2008.03.014

5. Zaky, R.R., Hessien, M.M., El-Midany, A.A., Khedr, M.H., Abdel-Aal, E.A., El-Barawy, K.A.: Preparation of silica nanoparticles from semi-burned rice straw ash. Powder Technol. 185, 31–35 (2008). doi:https://doi.org/10.1016/j.powtec.2007.09.012

6. Jesionowski, T.: Synthesis and characterization of spherical silica precipitated via emulsion route. J. Mater. Process. Technol. 203, 121–128 (2008). doi:https://doi.org/10.1016/j.jmatprotec.2007.10.008

7. Bernardos, A., Kourimská, L.: Applications of mesoporous silica materials in food - A review. Czech J. Food Sci. 31, 99–107 (2013). doi:10.17221/240/2012-CJFS

8. Wu, G., Wang, J., Shen, J., Yang, T., Zhang, Q., Zhou, B., Deng, Z., Bin, F., Zhou, D., Zhang, F.: Properties of sol–gel derived scratch-resistant nano-porous silica films by a mixed atmosphere treatment. J. Non. Cryst. Solids. 275, 169–174 (2000). doi:https://doi.org/10.1016/S0022-3093(00)00257-X

9. Tomozawa, M., Kim, D.-L., Lou, V.: Preparation of high purity, low water content fused silica glass. J. Non. Cryst. Solids. 296, 102–106 (2001). doi:https://doi.org/10.1016/S0022-3093(01)00877-8

10. Liu, C. li, Zheng, S. li, Ma, S. hua, Luo, Y., Ding, J., Wang, X. hui, Zhang, Y.: A novel process to enrich alumina and prepare silica nanoparticles from high-alumina fly ash. Fuel Process. Technol. 173, 40–47 (2018). doi:10.1016/j.fuproc.2018.01.007

11. Fardad, M.A.: Catalysts and the structure of SiO_2 sol-gel films. J. Mater. Sci. 35, 1835–1841 (2000). doi:10.1023/A:1004749107134

12. Kortesuo, P., Ahola, M., Karlsson, S., Kangasniemi, I., Yli-Urpo, A., Kiesvaara, J.: Silica xerogel as an implantable carrier for controlled drug delivery—evaluation of drug distribution and tissue effects after implantation. Biomaterials. 21, 193–198 (2000). doi:https://doi.org/10.1016/S0142-9612(99)00148-9

13. Sarawade, P.B., Kim, J.K., Hilonga, A., Kim, H.T.: Preparation of hydrophobic mesoporous silica powder with a high specific surface area by surface modification of a wet-gel slurry and spray-drying. Powder Technol. 197, 288–294 (2010). doi:10.1016/j.powtec.2009.10.006

14. Abou Rida, M., Harb, F.: Synthesis and Characterization of Amorphous Silica Nanoparticles from Aqueous Silicates Using Cationic Surfactants. Journal of Metals, Materials and Minerals. 24, 37–42 (2014).

15. Zulfiqar, U., Subhani, T., Husain, S.W.: Synthesis of silica nanoparticles from sodium silicate under alkaline conditions. J. Sol-Gel Sci. Technol. 77, 753–758 (2016). doi:10.1007/s10971-015-3950-7

16. Nistor, C., Ianchis, R., Ghiurea, M., Nicolae, C.-A., Spataru, C.-I., Culita, D., Pandele Cusu, J., Fruth, V., Oancea, F., Donescu, D.: Aqueous dispersions of silica stabilized with oleic acid obtained by Green Chemistry. Nanomaterials. 6, 9 (2016). doi:10.3390/nano6010009

17. Bagramyan, V. V, Sarkisyan, A.A., Ponzoni, C., Rosa, R., Leonelli, C.: Microwave Assisted Preparation of Sodium Silicate Solutions from Perlite. Theor. Found. Chem. Eng. 49, 731–735 (2015). doi:10.1134/S0040579515050048

18. Fertani-Gmati, M., Brahim, K., Khattech, I., Jemal, M.: Thermochemistry and kinetics of silica dissolution in NaOH solutions: Effect of the alkali concentration. Thermochim. Acta. 594, 58–67 (2014). doi:10.1016/j.tca.2014.09.003

19. Fertani-Gmati, M., Jemal, M.: Thermochemical and kinetic investigations of amorphous silica dissolution in NaOH solutions. J. Therm. Anal. Calorim. 123, 757–765 (2016). doi:10.1007/s10973-015-4980-7

20. Kalapathy, U., Proctor, A., Shultz, J.: A simple method for production of pure silica from rice hull ash. Bioresour. Technol. 73, 257-262 (2000).

21. Tong, K.T., Vinai, R., Soutsos, M.N.: Use of Vietnamese rice husk ash for the production of sodium silicate as the activator for alkali-activated binders. J. Clean. Prod. 201, 272–286 (2018). doi:10.1016/j.jclepro.2018.08.025

22. Affandi, S., Setyawan, H., Winardi, S., Purwanto, A., Balgis, R.: A facile method for production of high-purity silica xerogels from bagasse ash. Adv. Powder Technol. 20, 468–472 (2009). doi:10.1016/j.apt.2009.03.008

23. Gao, G., Zou, H., Gan, S., Liu, Z., An, B., Xu, J., Li, G.: Preparation and properties of silica nanoparticles from oil shale ash. Powder Technol. 191, 47–51 (2009). doi:10.1016/j.powtec.2008.09.006

24. Guo, Y., Zhao, Z., Zhao, Q., Cheng, F.: Novel process of alumina extraction from coal fly ash by pre-desilicating - Na_2CO_3 activation - Acid leaching technique. Hydrometallurgy. 169, 418–425 (2017). doi:10.1016/j.hydromet.2017.02.021

25. Bai, G., Teng, W., Wang, X., Zhang, H., Xu, P.: Processing and kinetics studies on the alumina enrichment of coal fly ash by fractionating silicon dioxide as nano particles. Fuel Process. Technol. 91, 175–184 (2010). doi:10.1016/j.fuproc.2009.09.010

26. Halina, M., Ramesh, S., Yarmo, M.A., Kamarudin, R.A.: Non-hydrothermal synthesis of mesoporous materials using sodium silicate from coal fly ash. Mater. Chem. Phys. 101, 344–351 (2007). doi:10.1016/j.matchemphys.2006.06.007

27. Kaduku, T., Daramola, M.O., Obazu, F.O., Iyuke, S.E.: Synthesis of sodium silicate from South African coal fly ash and its use as an extender in oil well cement applications. J. South. African Inst. Min. Metall. 115, 1175–1182 (2015). doi:10.17159/2411-9717/2015/v115n12a5

28. van der Merwe, E.M., Prinsloo, L.C., Mathebula, C.L., Swart, H.C., Coetsee, E., Doucet, F.J.: Surface and bulk characterization of an ultrafine South African coal fly ash with reference to polymer applications. Appl. Surf. Sci. 317, 73-83 (2014). doi:10.1016/j.apsusc.2014.08.080

29. Doucet, F.J., Mohamed, S., Neyt, N., Castleman, B.A., van der Merwe, E.M.: Thermochemical processing of a South African ultrafine coal fly ash using ammonium sulphate as extracting agent for aluminium extraction. Hydrometallurgy. 166, 174-184 (2016). doi:10.1016/j.hydromet.2016.07.017

30. Verbaan, B., Louw, G.K.E.: A Mass and Energy Balance Model for the Leaching of a Pulverised Fuel Ash in Concentrated Sulphuric Acid, Hydrometallurgy. 21, 305–317 (1989).

31. Daimon, K., Kato, E.: Morphology of corundum crystallized by heating mixture of ≠-Al_2O_3 and AlF_3. J. Cryst. Growth. 75, 348–352 (1986). doi:10.1016/0022-0248(86)90049-7

32. Dash, B., Das, B.R., Tripathy, B.C., Bhattacharya, I.N., Das, S.C.: Acid dissolution of alumina from waste aluminium dross. Hydrometallurgy. 92, 48–53 (2008). doi:10.1016/j.hydromet.2008.01.006

33. van der Merwe, E.M., Gray, C.L., Castleman, B.A., Mohamed, S., Kruger, R.A., Doucet, F.J.: Ammonium sulphate and/or ammonium bisulphate as extracting agents for the recovery of aluminium from ultrafine coal fly ash. Hydrometallurgy. 171, 185–190 (2017). doi:10.1016/j.hydromet.2017.05.015

34. Shemi, A., Mpana, R.N., Ndlovu, S., Van Dyk, L.D., Sibanda, V., Seepe, L.: Alternative techniques for extracting alumina from coal fly ash. Miner. Eng. 34, 30–37 (2012). doi:10.1016/j.mineng.2012.04.007

35. Musyoka, N.M., Petrik, L.F., Balfour, G., Gitari, W.M., Hums, E.: Synthesis of hydroxy sodalite from coal fly ash using waste industrial brine solution. J. Environ. Sci. Heal. - Part A Toxic/Hazardous Subst. Environ. Eng. 46, 1699–1707 (2011). doi:10.1080/10934529.2011.623961

36. Du Plessis, P.W., Ojumu, T. V., Petrik, L.F.: Waste minimization protocols for the process of synthesizing zeolites from South African coal fly ash. Materials. 6, 1688–1703 (2013). doi:10.3390/ma6051688

37. Nugteren, H.W., Moreno, N., Sebastia, E., Querol, X.: Determination of the Available Si and Al from Coal Fly Ashes under Alkaline Conditions with the Aim of Synthesizing Zeolite Products, in: 2001 International Ash Utilization Symposium, Center for Applied Energy Research, University of Kentucky. http://www.flyash.info/2001/newprod1/71nugter.pdf (2001).

38. Bhukari, S.S.R.: Microwave and Ultrasound Assisted Zeolitization of Coal Fly Ash, The University of Western Ontario. PhD thesis. https://ir.lib.uwo.ca/etd/3997 (2016).

39. Sedres, G.: Recovery of SiO_2 and Al_2O_3 from coal fly ash, University of Western Cape. MSc thesis. http://etd.uwc.ac.za/xmlui/handle/11394/5651 (2016).

40. Stanley, R., Samson Nesaraj, A.: Effect of Surfactants on the Wet Chemical Synthesis of Silica Nanoparticles. Int. J. Appl. Sci. Eng. 12, 9–21 (2014)

41. Singh, L.P., Bhattacharyya, S.K., Mishra, G., Ahalawat, S.: Functional role of cationic surfactant to control the nano size of silica powder. Appl. Nanosci. 1, 117–122 (2011). doi:10.1007/s13204-011-0016-1

42. Zulkifli, N.S.C., Ab Rahman, I., Mohamad, D., Husein, A.: A green sol-gel route for the synthesis of structurally controlled silica particles from rice husk for dental composite filler. Ceram. Int.

39, 4559–4567 (2013). doi:10.1016/j.ceramint.2012.11.052

43. Silica nanoparticles, Sigma Aldrich Product No 748161. https://www.sigmaaldrich.com/catalog/product/aldrich/748161?lang=en&region=ZA (2018). (accessed November 13, 2018).

44. Tchadjie, L.N., Ekolu, S.O.: Enhancing the reactivity of aluminosilicate materials toward geopolymer synthesis. J. Mater. Sci. 53, 4709–4733 (2018). doi:10.1007/s10853-017-1907-7

45. Falayi, T., Okonta, N.F., Ntuli, F.: Desilication of fly ash and development of lightweight construction blocks from alkaline activated desilicated fly ash. Int. J. Environ. Waste Manag. 20, 233–253 (2017). doi:10.1504/IJEWM.2017.087152

Supplementary material

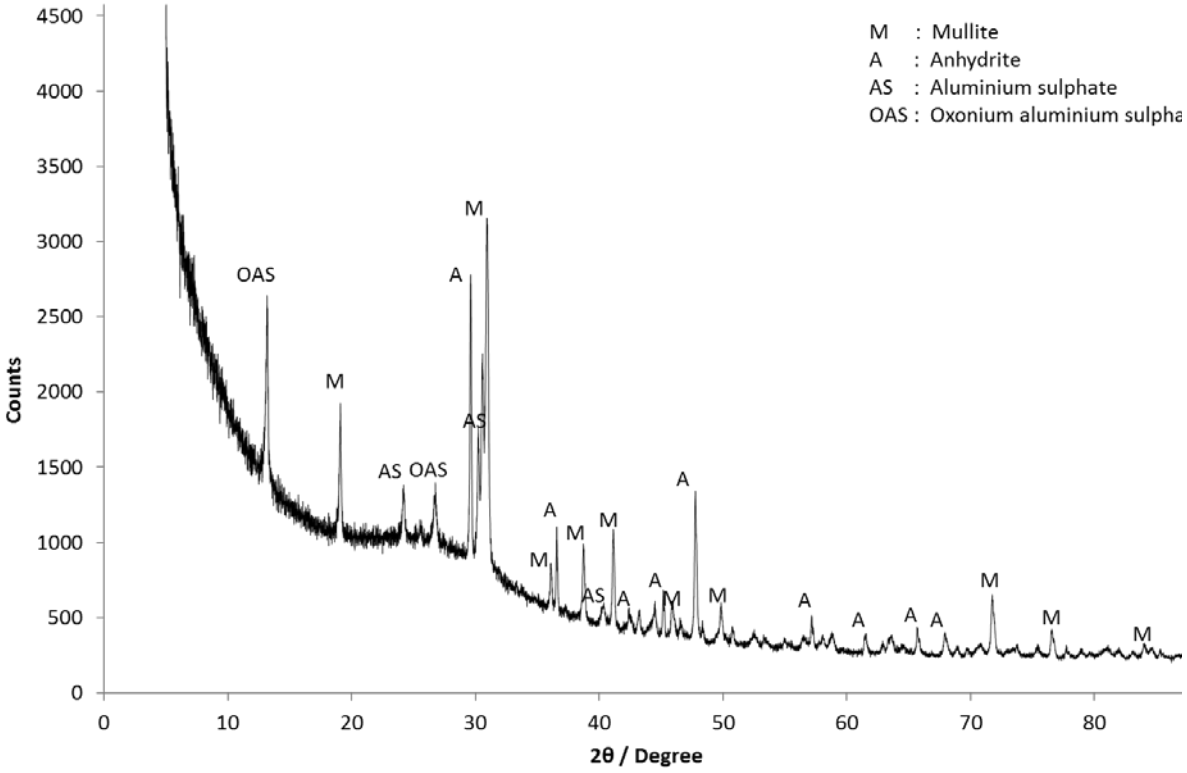

Figure S1. XRD analysis of unwashed $CFA_{Ac\text{-}sq}$.

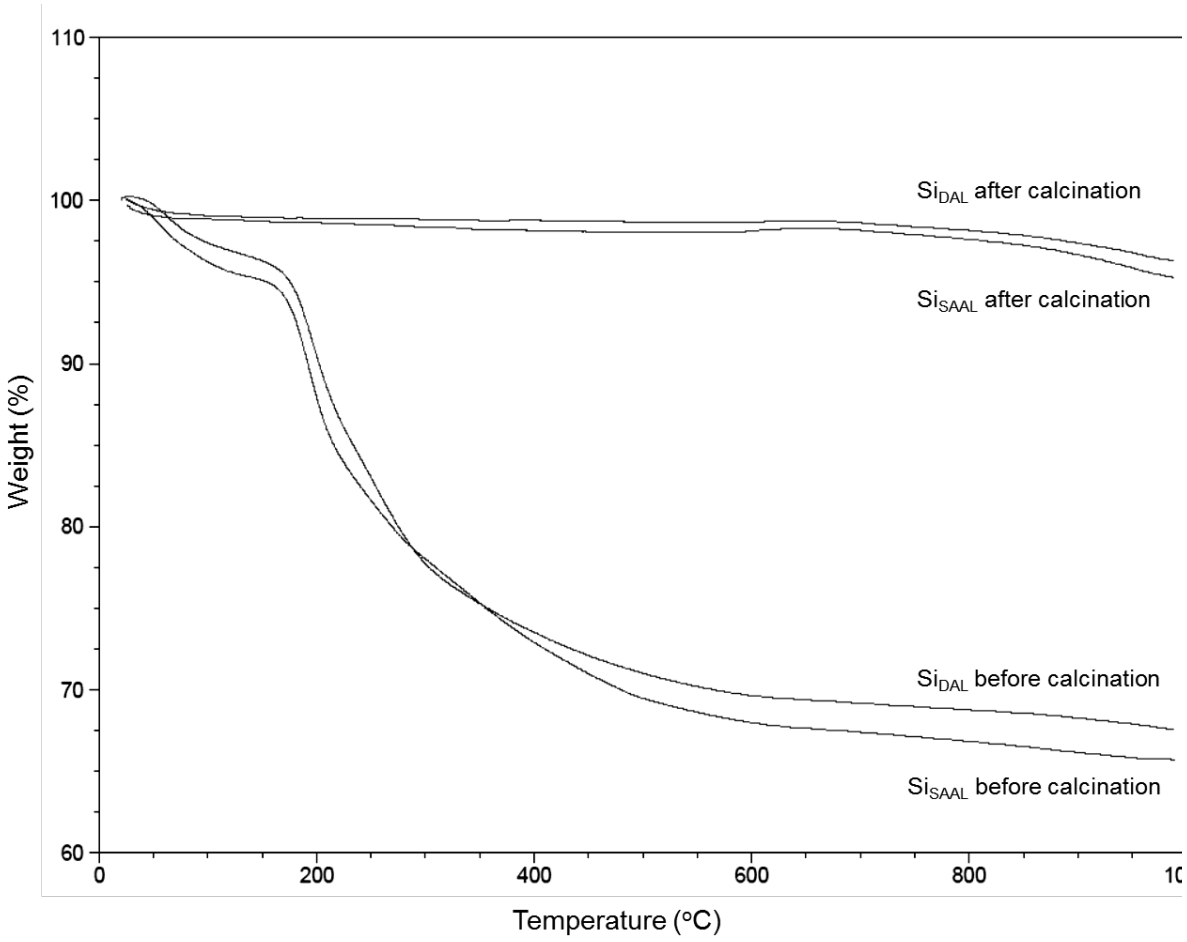

Figure S2. TGA analysis of silica nanoparticles, Si_{SAAL} and Si_{DAL}, before and after calcination.

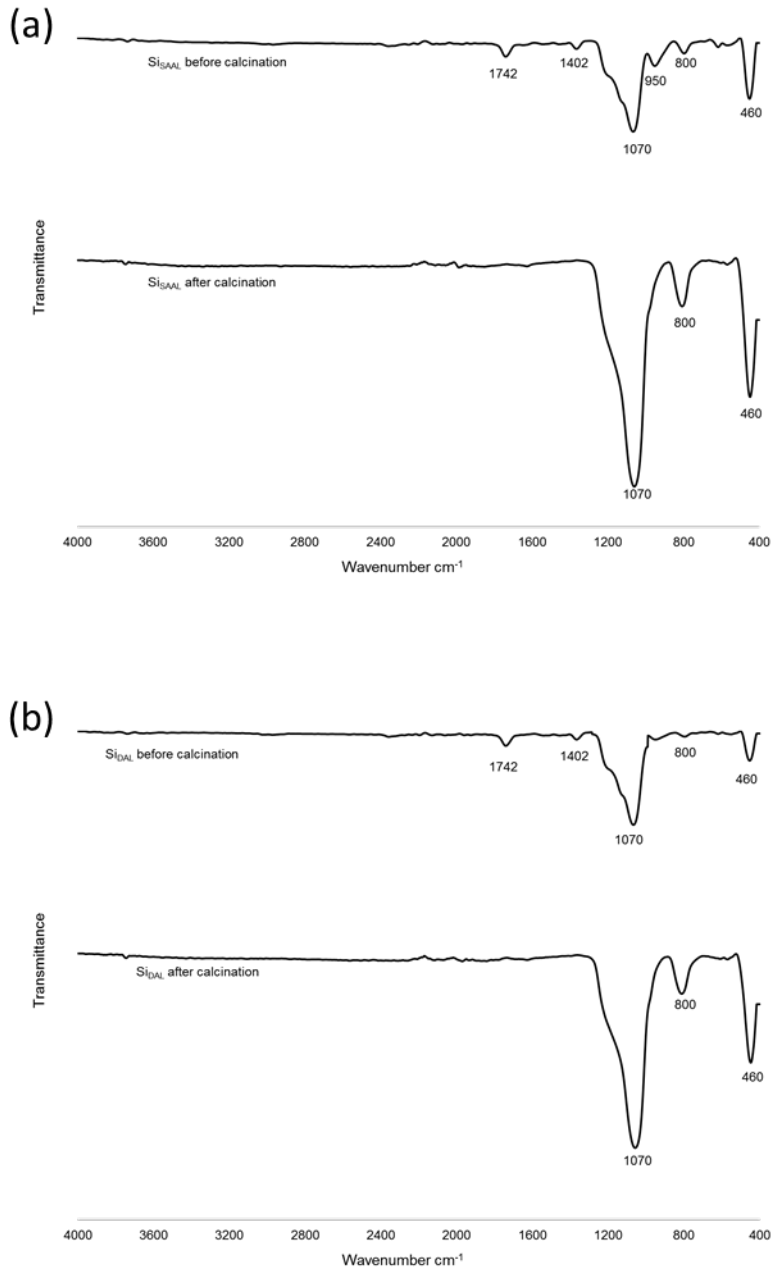

Figure S3. FTIR analysis of silica nanoparticles, Si_{SAAL} and Si_{DAL} before and after calcination.